Collimation, Acceleration, and Recollimation Shock in the Jet of Gamma-Ray Emitting Radio-loud Narrow-line Seyfert 1 Galaxy 1H0323+342

Kazuhiro Hada[1,2] , Akihiro Doi[3] , Kiyoaki Wajima[4] , Filippo D'Ammando[5] , Monica Orienti[5], Marcello Giroletti[5] ,
Gabriele Giovannini[5,6], Masanori Nakamura[7] , and Keiichi Asada[7]

[1] Mizusawa VLBI Observatory, National Astronomical Observatory of Japan, Osawa, Mitaka, Tokyo 181-8588, Japan; kazuhiro.hada@nao.ac.jp
[2] Department of Astronomical Science, The Graduate University for Advanced Studies (SOKENDAI), 2-21-1 Osawa, Mitaka, Tokyo 181-8588, Japan
[3] Institute of Space and Astronautical Science, Japan Aerospace Exploration Agency, 3-1-1 Yoshinodai, Chuo, Sagamihara 252-5210, Japan
[4] Korea Astronomy and Space Science Institute (KASI), 776 Daedeokdae-ro, Yuseong-gu, Daejeon 305-348, Republic of Korea
[5] INAF Istituto di Radioastronomia, via Gobetti 101, I-40129 Bologna, Italy
[6] Dipartimento di Fisica e Astronomia, Università di Bologna, via Ranzani 1, I-40127 Bologna, Italy
[7] Institute of Astronomy & Astrophysics, Academia Sinica, 11F of Astronomy-Mathematics Building, AS/NTU No. 1, Taipei 10617, Taiwan
Received 2018 March 26; revised 2018 May 2; accepted 2018 May 10; published 2018 June 21

Abstract

We investigated the detailed radio structure of the jet of 1H 0323+342 using high-resolution multifrequency Very Long Baseline Array observations. This source is known as the nearest γ-ray emitting radio-loud narrow-line Seyfert 1 (NLS1) galaxy. We discovered that the morphology of the inner jet is well characterized by a parabolic shape, indicating that the jet is continuously collimated near the jet base. On the other hand, we found that the jet expands more rapidly at larger scales, resulting in a conical shape. The location of the "collimation break" is coincident with a bright quasi-stationary feature at 7 mas from core (corresponding to a deprojected distance on the order of $\sim$100 pc), where the jet width locally contracts together with highly polarized signals, suggesting a recollimation shock. We found that the collimation region is coincident with the region where the jet speed gradually accelerates, suggesting a coexistence of the jet acceleration and collimation zone, ending up with the recollimation shock, which could be a potential site of high-energy γ-ray flares detected by the *Fermi*-LAT. Remarkably, these observational features of the 1H 0323+342 jet are overall very similar to those of the nearby radio galaxy M87 and HST-1 as well as some blazars, suggesting that a common jet formation mechanism might be at work. Based on the similarity of the jet profile of the two sources, we also briefly discuss the mass of the central black hole of 1H 0323+342, which is also still highly controversial in this source and NLS1s in general.

Key words: galaxies: active – galaxies: individual (1H 0323+342) – galaxies: jets – galaxies: Seyfert –
gamma rays: galaxies – radio continuum: galaxies

1. Introduction

Narrow-line Seyfert 1 (NLS1) galaxies are a subclass of active galactic nuclei (AGNs). This class is defined by its optical properties, i.e., narrow permitted line FWHM (H$\beta < 2000$ km s^{-1}), [O III]/H$\beta < 3$, and a bump due to Fe II emission lines (Osterbrock & Pogge 1985). Based on these peculiar optical characteristics along with the large soft X-ray excess (e.g., Boller et al. 1996), NLS1s are suggested to have low black hole masses ($10^{6-8} M_\odot$) and high accretion rates (close to or above the Eddington limit), making this population a possible candidate for studying the physics of rapidly evolving supermassive black holes (SMBHs).

In recent years, this class of objects has attracted much attention in the high-energy astrophysical community; the discovery of γ-ray emission by the *Fermi* satellite from some radio-loud NLS1s suggested the presence of a possible third class of AGN with relativistic jets, in addition to blazars and radio galaxies (Abdo et al. 2009a, 2009b). The γ-ray emission from NLS1s is surprising and poses a challenge to our current understanding of jet formation, since NLS1s are generally thought to be hosted by spiral galaxies, which are not expected to produce high-power jets. To date, γ-ray emission has been detected in a dozen radio-loud NLS1s (D'Ammando et al. 2016; Paliya et al. 2018), and the ejection of superluminal features is detected in a few of them (D'Ammando et al. 2013; Lister et al. 2016). This further confirms that relativistic jets

constitute an essential channel of energy release at least in these active NLS1 nuclei.

Some pioneering VLBI studies on radio-loud NLS1s (Doi et al. 2006, 2007, 2011; Foschini et al. 2011; Giroletti et al. 2011; Orienti et al. 2012, 2015; Lister et al. 2016) revealed that the parsec-scale morphologies of radio-loud NLS1s are reminiscent of blazars, i.e., they consist of a bright compact core and one-sided jet. This implies that similar processes may be at work in producing γ-rays in blazars and γ-ray detected NLS1s, such as the Doppler boosting effect with small jet viewing angles. However, due to the lack of sufficient very large baseline interferometry (VLBI) studies so far, detailed parsec-scale structures of the NLS1s jets are still poorly understood. Direct constraints on the innermost jet properties from VLBI are complementary to what can be inferred from radio-to-γ-ray broadband spectral energy density (SED) modeling (Abdo et al. 2009b; Foschini et al. 2011; D'Ammando et al. 2012, 2013, 2014, 2015, 2016). Moreover, dedicated high-resolution studies of NLS1 jets may help understand the mechanisms of relativistic jet launching, collimation, and acceleration in a possible distinct (M_{BH}, $\dot{M}$) domain from blazars/radio galaxies that have been intensively investigated (e.g., Marscher et al. 2008; Asada & Nakamura 2012; Hada et al. 2013; Nagai et al. 2014; Gómez et al. 2015; Boccardi et al. 2016; Mertens et al. 2016; Giovannini et al. 2018; Nakahara et al. 2018).

In this paper, we focus on the famous NLS1 galaxy 1H 0323+342. This source is known as the nearest (a redshift of 0.063) γ-ray detected NLS1 (Abdo et al. 2009b), and is one of the few NLS1s where the host galaxy is imaged (Zhou et al. 2007), along with FBQS J1644+2619 (D'Ammando et al. 2017) and PKS 2004–447 (Kotilainen et al. 2017). Thus 1H 0323+342 is a unique target that allows us to probe the vicinity of the central engine at the highest linear resolution among γ-ray active NLS1s (i.e., 1 mas = 1.2 pc). The parsec-scale structure of the source was first examined by Wajima et al. (2014) with the Japanese VLBI Network and the Very Long Baseline Array (VLBA) at 2, 8, and 15 GHz, revealing a blazar-like one-sided core-jet structure toward the southeast. Kinematic properties of the parsec-scale jet were investigated by several authors (Wajima et al. 2014; Fuhrmann et al. 2016; Lister et al. 2016; Doi et al. 2018). The latter three papers reported highly superluminal features up to $\sim$9 c. In addition, Wajima et al. (2014), Fuhrmann et al. (2016), and Doi et al. (2018) found one or two quasi-stationary features at parsec scales that might be associated with standing shocks. Detailed radio-to-γ-ray broadband properties of the source are studied by Paliya et al. (2014), Yao et al. (2016), and Kynoch et al. (2018). Regarding the mass of the central BH, several independent measurements suggest $M_{BH} \sim 2 \times 10^7 M_\odot$ (Zhou et al. 2007; Wang et al. 2016; Yao et al. 2016; Landt et al. 2017), although this is still under active debate and some authors suggest a much higher black hole mass (a few times $10^8 M_\odot$; León Tavares et al. 2014).

In this paper, we report the result from our multifrequency VLBA observation of 1H 0323+342, which aims to better understand the parsec-to-subparsec-scale structures of this jet. In the next section we describe our observation and data reduction. In Sections 3 and 4, our results are presented and discussed. In the final section we summarize the paper. Throughout the paper we adopt cosmological parameters $H_0 = 70$ km s^{-1} Mpc^{-1}, $\Omega_M = 0.3$, and $\Omega_\Lambda = 0.7$. This corresponds to 1 mas = 1.2 pc at $z = 0.063$. Spectral index α is defined as $S_\nu \propto \nu^{+\alpha}$.

2. Observations and Data Reduction

We observed 1H 0323+342 with VLBA on 2016 January 2. The observations were made at nine frequencies of 1.4/1.7 GHz (L-band), 2.3/8.4 GHz (S/X bands), 5 GHz (C-band), 12/15 GHz (U-band), 24 GHz (K-band), and 43 GHz (Q-band) in a 11 hr continuous run. The receiver at each frequency band was alternated in turn every 10–30 minutes. The observation involved rapid switching between the target and the nearby radio source 0329+3510 (separated by 1°36 on the sky) to allow phase-referencing and relative astrometry between the two sources. Some short scans on the bright source 3C 84 were also inserted as a fringe finder and bandpass calibrator. The observation was made in dual (left-/right-hand circular) polarization mode. The received signals were sampled with 2-bit quantization and recorded at an aggregate rate of 2 Gbps (a total bandwidth of 512 MHz) using the digital-down-converter-4 (DDC-4) wideband recording mode. The down-converted signals were divided into four 64 MHz sub-bands in each polarization.

The initial data calibration was performed using the National Radio Astronomy Observatory Astronomical Image Processing System (AIPS) based on the standard VLBI data reduction procedures. The amplitude calibration was made with opacity corrections using the measured system noise temperature and the elevation-gain curve of each antenna. We next performed a priori corrections for the visibility phases; antenna parallactic angle differences between 1H 0323+342 and 0329+3510, ionospheric dispersive delays using the ionospheric model provided by the Jet Propulsion Laboratory, and instrumental delays/phases using a scan of 3C 84 were corrected. Then, to create images of these sources, we performed a fringe-fitting on each source separately and removed residual delays, rates, and phases assuming a point source model. Images were created in the DIFMAP software (Shepherd 1997) with iterative phase/amplitude self-calibration.

In this paper, we primarily focus on total-intensity results. Our dedicated multifrequency polarimetric study based on these data will be presented in a forthcoming paper.

3. Results

3.1. Multifrequency Images

In Figure 1 we show VLBA images of 1H 0323+342 obtained at the nine frequencies. The image parameters obtained for these maps are listed in Table 1. At all the frequencies, a core-jet structure is seen, and the one-sided jet is elongated toward the southeast (P.A. $\sim$125°). The overall jet morphology at 8/12/15 GHz is very similar to the previous VLBA 8/15 GHz images presented by Wajima et al. (2014), Fuhrmann et al. (2016), and Doi et al. (2018). Wajima et al. (2014) and Doi et al. (2018) reported a quasi-stationary bright feature at $\sim$7 mas downstream of the core. The corresponding feature consistently exists also in our 8/12/15 GHz images, indicating that the feature is still present after more than 5–10 years. We here call this feature "S."

At low frequencies, feature S is more prominent, becoming the brightest component in the 1.4 GHz image. The low-frequency images also reveal the downstream jet emission, which extends $\sim$60–80 mas from the core. In contrast, the source structure at 24 and 43 GHz becomes more compact and is mostly core dominated.

We stress that this is the first VLBI result on 1H 0323+342 up to 43 GHz where the highest resolution and transparency to the jet base is attained. To quantify the innermost radio core at 43 GHz, we fit the calibrated visibility data with an elliptical Gaussian model using the DIFMAP task `modelfit`. Our best-fit result is summarized in Table 2. With these values and Equation (1) in Wajima et al. (2014), the brightness temperature of the 43 GHz core is estimated to be $T_B = 5.3 \times 10^{10}$ K. The value is very similar to those reported by Wajima et al. (2014) at low frequencies.

Wajima et al. (2014) and Fuhrmann et al. (2016) reported another quasi-stationary feature around 0.3–0.5 mas from the core in their multi-epoch 8/15 GHz images. Here we searched for the corresponding feature in our images at 8, 12, 15, 24, and 43 GHz. However, the jet intensity profile around 0.3–0.5 mas was more or less smooth in our images and we did not clearly find a feature like this.

3.2. Jet Width Profile

Measuring the profile of jet width $W(z)$ as a function of radial distance z provides important clues to the formation and collimation mechanisms of a relativistic jet, as demonstrated in recent VLBI studies on nearby radio galaxies (Asada & Nakamura 2012; Hada et al. 2013, 2016; Nakamura & Asada 2013; Boccardi et al. 2016; Tseng et al. 2016;
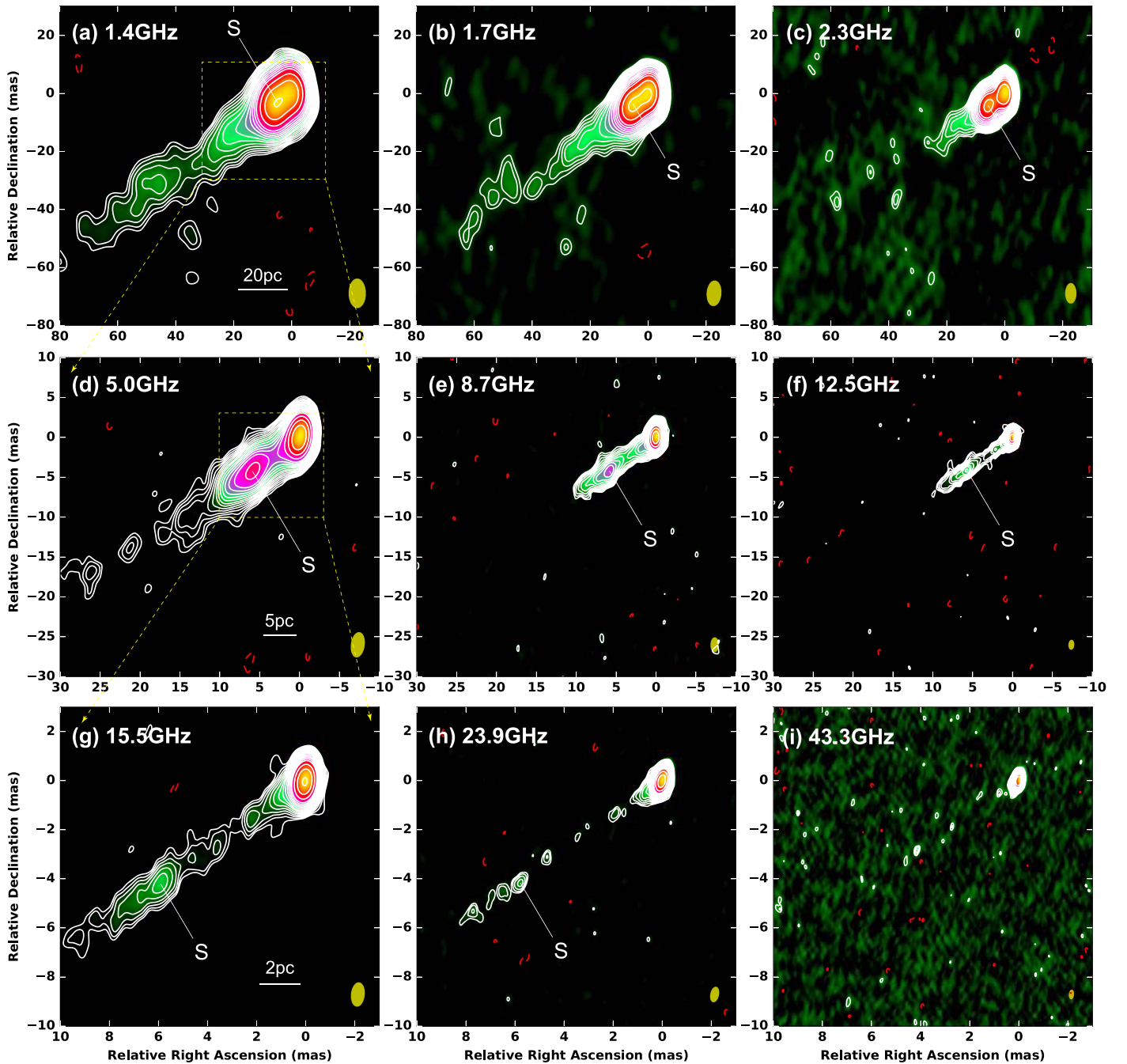
Figure 1. VLBA images of 1H 0323+342. (a), (b), (c), (d), (e), (f), (g), (h), and (i) are naturally weighted images at 1.4, 1.7, 2.3, 5.0, 8.7, 12.5, 15.5, 23.9, and 43.3 GHz, respectively. For each image, contours start from $-1, 1, 2, \ldots$ times a 3σ image rms level and increase by factors of $2^{1/2}$. The yellow ellipse in the bottom right corner of each map is the beam size of the map. Feature S is a quasi-stationary component located at 7 mas from the core.

Giovannini et al. 2018; Nakahara et al. 2018). Our multi-frequency images of 1H 0323+342 allow us to examine $W(z)$ of this jet in detail.

We basically followed the method described in our previous studies on M87 (Hada et al. 2013, 2016). We made transverse slices of the 1H 0323+342 jet every 1/2–1/3 of the beam size along the jet, and each slice was fit with a single Gaussian function (because the jet is single-ridged at all distances in our VLBA images[8]). We then defined the jet width at each z as a

deconvolved size of the fitted Gaussian $(\Theta_{\mathrm{Gauss}}^2 - \Theta_{\mathrm{beam}}^2)^{1/2}$, where Θ_{Gauss} and Θ_{beam} are the FWHM of the fitted Gaussian and the projected beam size perpendicular to the jet, respectively. The result is summarized in Figure 2, where the measured jet width profile is plotted as a function of projected (angular) distance from the innermost (43 GHz) core. Thanks to the wide frequency coverage, we could measure the jet width profile over ~3 orders of magnitude at distances from $\lesssim 0.1$ mas to ~80 mas.

Figure 2 reveals some very interesting features on the structure of this jet. The jet shows a clear change in the collimation slope between $z \lesssim 7$ mas and $z \gtrsim 7$ mas. We then fit a power-law function $W(z) = Az^a$ to the inner jet
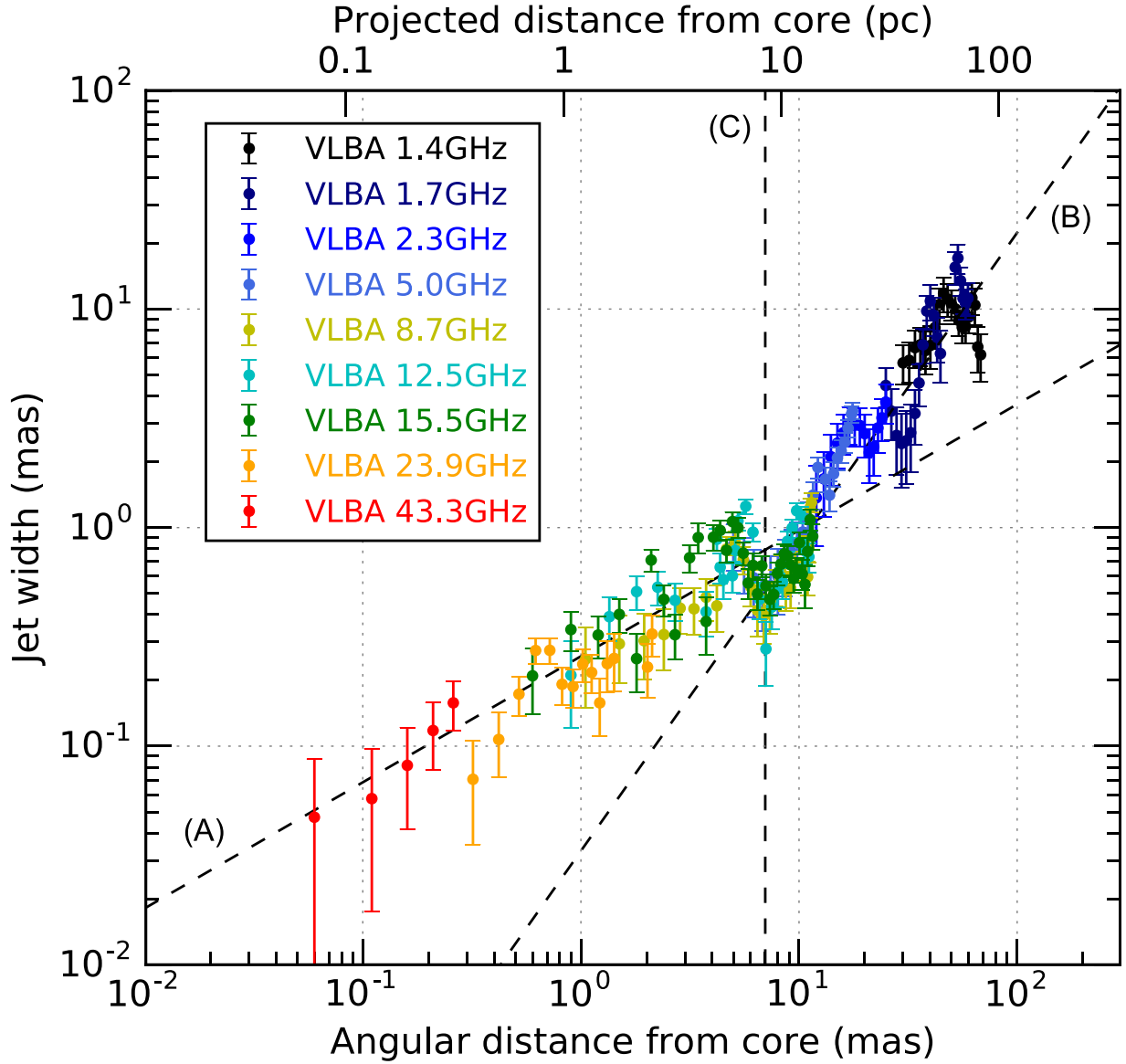
---

[8] Note that Doi et al. (2018) has recently revealed a limb-brightened jet profile around S based on a detailed image analysis of VLBA archival data. This does not affect the result of our jet-width measurement presented here.

Figure 2. Jet width profile $W(z)$ of 1H 0323+342 as a function of (projected) distance z from the 43 GHz core. The dashed line (A) represents a best-fit model for the inner ($z < 6.5$ mas) jet $W(z) \propto z^{0.58}$, indicating a parabolic collimating jet. The dashed line (B) represents a best-fit model for the outer ($z > 7.5$ mas) jet $W(z) \propto z^{1.41}$, indicating a hyperbolic expanding jet. The vertical dashed line (C) indicates the location of the quasi-stationary feature S, where the jet width locally shrinks (by a factor of 2) and the transition of jet shape occurs.

<table>
<tr><td colspan="4" align="center">Table 1
VLBA Observations of 1H 0323+342 in 2016 January</td></tr>
</table>

Frequency (GHz)	Beam Size (mas × mas, degree) (a)	I_p (mJy/bm) (b)	I_{rms} (mJy/bm) (c)
1.44	9.92 × 5.69, 0	135	0.085
1.70	8.58 × 4.84, −4	124	0.134
2.32	6.80 × 3.61, 0	146	0.193
5.00	3.09 × 1.64, −8	155	0.056
8.68	1.78 × 0.94, −2	177	0.141
12.5	1.14 × 0.64, −4	277	0.118
15.5	0.96 × 0.53, −6	283	0.144
23.9	0.61 × 0.32, −12	280	0.224
43.3	0.36 × 0.18, −5	242	0.318

Note. (a) Synthesized beam with naturally weighted scheme. (b) Peak intensity of the self-calibrated images of 1H 0323+342 under the naturally weighted scheme. (c) rms image noise level of 1H 0323+342 images under the naturally weighted scheme.

<table>
<tr><td colspan="4" align="center">Table 2
Modelfit Parameters for 43 GHz Core</td></tr>
</table>

θ_{maj} (μas) (a)	θ_{min} (μas) (b)	PA (degree) (c)	S_{core} (mJy) (d)
131 ± 9	60 ± 10	130 ± 3	294 ± 29

Note. (a) Major axis FWHM size of the derived elliptical Gaussian. (b) Minor axis FWHM size of the derived elliptical Gaussian. (c) Position angles of the major axes of the Gaussian model. (d) Total flux densities of the Gaussian models. (e) Combined visibility data over the two epochs. For (a), (b), and (c), a practical uncertainty of each parameter was estimated by comparing the difference of the derived results between modelfit in Difmap and JMFIT in AIPS. For (d), we adopt a 10% uncertainty based on the typical amplitude calibration accuracy.

data (0.1 mas $< z <$ 6.5 mas) and the outer jet data (7.5 mas $< z <$ 80 mas) separately (where A and a are free parameters). We found that the inner jet region within 7 mas is
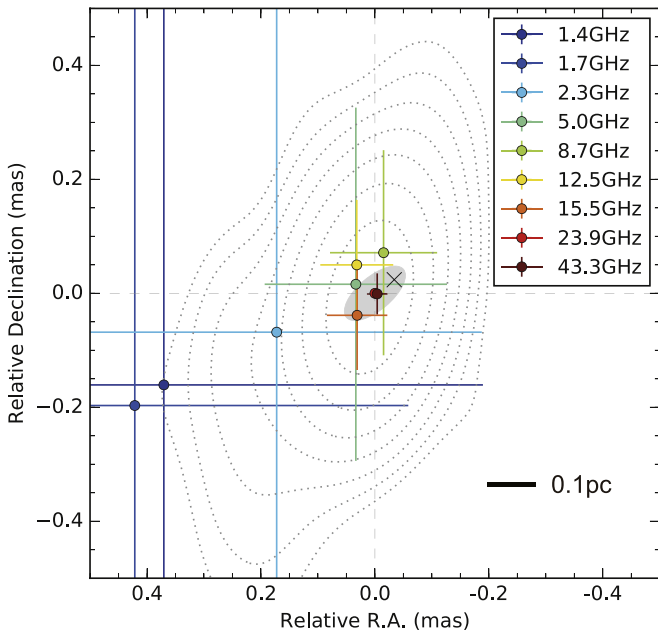
Figure 3. Astrometry of the core position of 1H 0323+342 at various frequencies. The position of the 24 GHz core is set to be the coordinate origin of this plot. Note that position of the 43 GHz core is almost identical to that of the 22 GHz core. The contours are a total-intensity map 1H 0323+342 at 43 GHz. The gray-shaded ellipse indicates a best-fit elliptical Gaussian model to the 43 GHz core (see Table 2). The cross indicates an extrapolated position z_0 of the origin of the parabolic jet (see Section 3.3), which is a likely position of the central black hole.

Figure 4. Spectral index (defined as $S_\nu \propto \nu^{+\alpha}$) distribution of 1H 0323+342 for various frequency pairs (color maps): (A) between 2.3 and 5.0 GHz, (B) between 8.7 and 15.5 GHz, (C) 15.5 and 23.9 GHz, and (D) 23.9 and 43.3 GHz. Contours in each inset are a total-intensity map at the lower frequency, starting from $(1, 2, 4, 8, 16, 32, 64, \ldots)$ times 0.2 mJy beam^{-1}. The yellow ellipse in each inset is the size of the convolving beam.

well described by a parabolic shape with $a = 0.58 \pm 0.02$, indicating that the jet is continuously collimated over these distances. On the other hand, beyond 7 mas, the jet starts to expand more rapidly with $a = 1.41 \pm 0.02$, suggesting a conical or hyperbolic expansion. This parabolic-to-conical/hyperbolic transition occurs exactly at 7 mas from the core, where the bright stationary component S is located. The jet width at 7 mas (on the stationary component) locally shrinks by a factor of 2. The local contraction at S has recently been reported by Doi et al. (2018) based on MOJAVE 15 GHz data, and our result further confirms this feature. All of the findings reported here are robust thanks to the sufficient number of data sets and consistency at different frequencies. It is notable that the observed jet collimation profile looks very similar to that seen in the nearby radio galaxy M87 and HST-1 (Asada & Nakamura 2012). We discuss the comparison between M87 and 1H 0323+342 in Section 4.

3.3. Core Shift

Our multifrequency VLBA data also enable us to examine the core shift (e.g., Lobanov 1998; Hada et al. 2011) of 1H 0323+342. We investigated the core shift of the source in the following way. Between 24 and 43 GHz, the core shift of the target was measured with respect to the calibrator 0329+3510[9] by using the phase-referenced images of 0329+3510. On the other hand, between 1.4 and 24 GHz, the complex structure of the calibrator prevented us from obtaining reliable core-shift measurements (see the Appendix). Instead,

---

[9] In this case, the core shift from the calibrator may affect the measurement of the core shift of the target, but we confirmed that the calibrator core-shift between 24 and 43 GHz is negligible (see the Appendix for details).
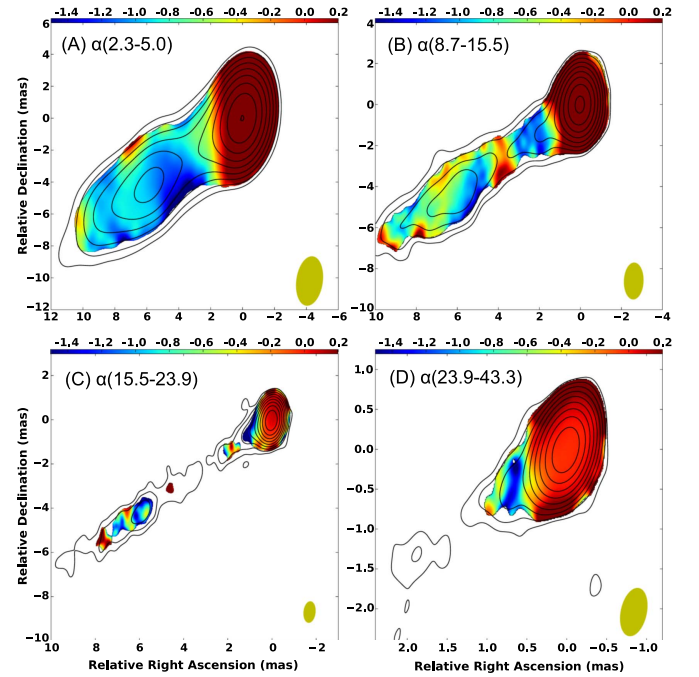
we performed a "self-referencing" method at these frequencies because 1H 0323+342 shows a well-defined optically thin feature S at ~7 mas from the core. We thus measured the core shift between 1.4 and 24 GHz by assuming that the feature S has no frequency-dependent position shifts.

The result of our core-shift measurement is shown in Figure 3. The origin of this plot is set to be the core position at 24 GHz, at which core-shift measurements could be made with respect to all the other frequencies. The (x, y) position errors for each data are one-tenth of the beam size, which is rather conservative. Interestingly, the measured core positions between 5.0 and 43 GHz were concentrated within the central ~100 μas area, and we did not find any clear trend of the core shift among these frequencies. At 2.3 GHz and the lower frequencies, Figure 3 implies a possible trend of the core shift in the direction of the jet, but the position uncertainties of the low-frequency cores are quite large due to the poor angular resolution and the severe blending between the core and neighboring jet emission. Therefore, we conclude that the core shift $\Delta\theta_{cs}$ of 1H 0323+342 is very small: $\Delta\theta_{cs} \lesssim 100$ μas between 5.0 and 43 GHz and $\Delta\theta_{cs} \lesssim 500$ μas between 1.4 and 43 GHz.

Given that the radio core shows an optically thick spectrum (see Section 3.4), the small core shift suggests that the jet has a small viewing angle toward our line of sight. This is consistent with the detection of highly superluminal components up to ~9 c (Lister et al. 2016), which constrains $\theta_{view} \lesssim 12°$. An even smaller viewing angle $\theta_{view} \lesssim 4°$ is suggested when the radio variability timescales are additionally considered (Fuhrmann et al. 2016).

The small core shift and viewing angle imply that the angular separation of the central BH with respect to the radio core is rather short. Such a separation can be measured if the
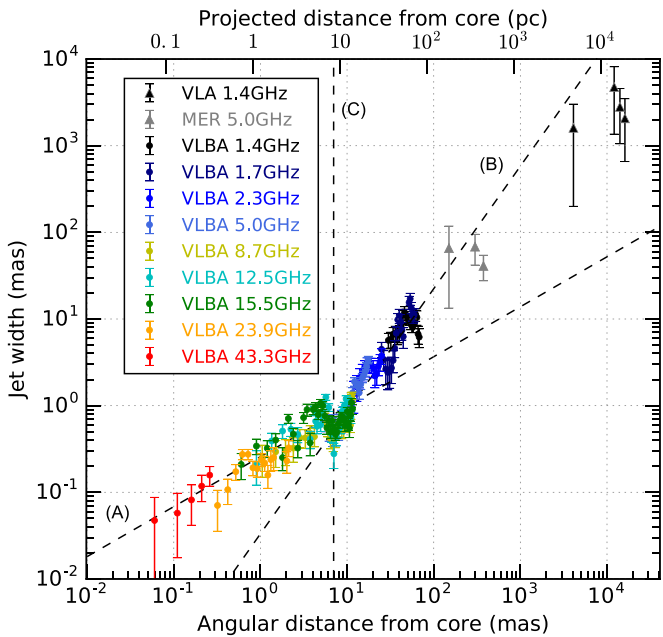
Figure 5. Extended plot of the jet width profile of 1H 0323+342 including MERLIN and VLA measurements at large scales. The dashed lines (A), (B), and (C) are the same as in Figure 2.

Figure 6. VLBA 15 GHz polarization map of 1H 0323+342. We retrieved the calibrated data from the MOJAVE 15 GHz archive. The total intensity distribution is shown by contours, while the fractional polarization distribution is shown by color (the values are in percent). Note that the EVPA shown are not RM-corrected.

frequency dependence of the core shift is accurately determined (Hada et al. 2011), while the accuracy of our core-shift measurements on 1H 0323+342 does not suffice to use this method. Instead, we can reasonably deduce the BH position by taking advantage of the observed parabolic profile of the inner jet. Assuming that the parabolic shape continues all the way down to the BH and the jet width converges to zero at the BH position, we again fit the inner jet within $z < 6.5$ mas using the following equation (instead of $W = Az^a$):

$$W(z) = A(z - z_0)^a, \qquad (1)$$

where the additional free parameter z_0 is the angular distance of the BH position from the 43 GHz core. We obtained a very similar parabolic profile $a = 0.60 \pm 0.03$ together with $z_0 = -41 \pm 36$ μas. As visualized in Figure 3, the derived BH position z_0 (as shown by the cross) is within the ellipse of the 43 GHz core. Thus the parabolic jet shape consistently suggests a small viewing angle of this jet. For $\theta_{\rm view} = 4°–12°$, the deprojected distance between the 43 GHz core and the BH position is estimated to be ∼(0.24–0.71)pc. Note that z_0 might be an upper limit of the BH-core distance if the (parabolic) jet has a non-zero width at the BH position.

3.4. Spectra

In Figure 4, we show maps of spectral index distribution of 1H 0323+342 for various frequency pairs. To create an accurate spectral index map for each frequency pair, map positions at the two frequencies were adjusted by using the astrometric results in Section 3.3. In Figure 4, we also used the same uv range and pixel sampling for each frequency pair. Then the two maps were convolved with a synthesized beam at the lower frequency.

As seen in Figure 4, the core regions generally show flat-to-inverted (i.e., optically thick) spectra, while the extended jet regions show steep (optically thin) spectra, which is consistent
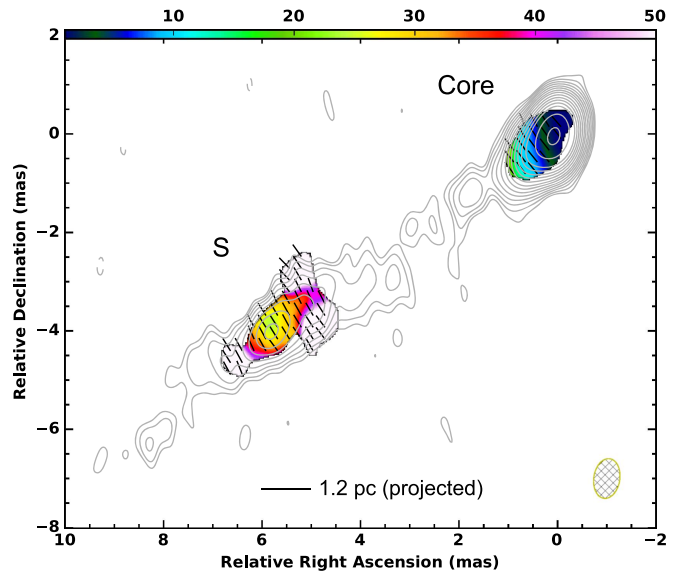
with typical characteristics of blazar jets. Some previous studies suggest that radio spectra of NLS1 jets are similar to those in young radio galaxies (e.g., Gallo et al. 2006; Berton et al. 2016a), whose spectral turnover occurs around 1–10 GHz. However, our result indicates that the radio spectra of the 1H 0323+342 core remain flat even at 43 GHz.

Regarding the extended jet, there is a possible trend that the spectra on and right down the quasi-stationary feature S are slightly flatter than those in the upstream side of S. Although the uncertainties are still large, this might indicate re-energization of nonthermal electrons via shock in the feature S.

4. Discussion

4.1. Jet Collimation Break at the Recollimation Shock

Structural transition of jet profile has recently been discovered in some nearby radio galaxies (M87; Asada & Nakamura 2012, NGC 6251; Tseng et al. 2016, 3C 273; Akiyama et al. 2018, NGC 4261; Nakahara et al. 2018). This has triggered an active discussion about the mechanisms of jet formation and collimation. Our result presented here is the first example where such a structural transition was discovered in the jet of a NLS1 galaxy.

To check the jet collimation profile beyond the VLBI scales, we additionally analyzed a few archival data of 1H 0323+342 obtained by connected radio interferometers. We found one VLA data set at 1.4 GHz (Project ID AM601, obtained in 1998 with the B configuration and an on-source time of 15 minutes) and another data with MERLIN at 5 GHz (obtained in 2006 with an on-source time of 5 minutes). At large scales, the main jet can continuously be seen up to ∼10–20 arcsec from the core, while the overall source morphology shows a hint of the counter jet (see also Antón et al. 2008).[10] In Figure 5 we show an extended plot of the jet width profile (for the main jet)

---

[10] A more detailed study on the kiloparsec-scale structure of this jet will be presented in a forthcoming paper (A. Doi et al. 2018, in preparation).

including the VLA/MERLIN measurements. Beyond 100 mas from the core, the deviation from the inner jet parabola is more evident, and the jet width becomes a factor of $\gtrsim 10$ wider than that expected from the parabolic profile.[11] If we fit the width profile of the outer jet ($z > 7.5$ mas) together with the VLBA, MERLIN, and VLA data, a best-fit slope results in $a = 1.25 \pm 0.02$, approaching a conical shape.

The observed jet width profile strongly suggests that the structural transition from parabolic to hyperbolic/conical originates in the quasi-stationary feature S. This situation is remarkably similar to the case of the jet in M87 (Asada & Nakamura 2012), where its parabolic-to-conical transition occurs at the bright quasi-stationary (and possibly γ-ray emitting) knot HST-1 located at ~ 120 pc from the nucleus. For HST-1, its cross section seems to be slightly smaller than expected from the parabolic profile. This leads to an argument that HST-1 represents a recollimation shock at the end of the collimation zone (Cheung et al. 2007; Asada & Nakamura 2012).

For 1H 0323+342, the local contraction of the jet width at the transition site is more evident than in HST-1. This feature was first reported by Doi et al. (2018), and our multifrequency study further confirmed this. While in M87 there is still no clear evidence for the "recollimation zone" between the parabolic region and HST-1, in 1H 0323+342 we can clearly see the recollimation zone just upstream of S ($z \sim 6$–7 mas), connecting the whole sequence of parabolic zone, recollimation zone, shock, and expansion. The rebrightening of jet intensity with a possible spectral flattening at S indicates the re-energization of jet particles via shock compression. Interestingly, the deprojected distance of the feature S is ~ 40–120 pc (for $\theta_{\text{view}} \sim 4°$–12°), which is similar to that of HST-1 in parsecs. Moreover, S seems to be caused by the passage of highly superluminal components (Doi et al. 2018, see also Section 4.2), and this type of event is repeatedly seen also in HST-1 (Biretta et al. 1999; Cheung et al. 2007; Giroletti et al. 2012; Hada et al. 2015). We therefore suggest that the feature S in 1H 0323+342 is analogous to HST-1 in M87, and might be a potential site of γ-ray emission (see Section 4.3).

We further checked one recent VLBA polarization map taken by the MOJAVE 15 GHz program to search for any polarimetric feature associated with S (Figure 6). Interestingly, the jet exhibits strongly polarized emission exactly on S, where the values of fractional polarization reach as high as $\sim 30\%$, indicating the presence of highly ordered magnetic fields. This is in agreement with S being a shocked compressed feature. Note that the apparent electric-vector-polarization angles (EVPA) in both the core and S are perpendicular to the jet, but the EVPA shown are not rotation-measure (RM)-corrected ones, preventing us from discussing the intrinsic geometry of the B fields associated with the jet. A recent optical polarimetry study on this source suggests that the optical EVPA is parallel to the jet axis (Itoh et al. 2014), implying that the B-field direction (associated with the optical emission) is perpendicular to the jet. Thus a future dedicated VLBI polarimetric study

---

[11] There is a possibility that the jet viewing angle is different between parsec and kiloparsec scales since the position angle of the kiloparsec-scale jet is $\sim 90°$ (Antón et al. 2008), while the parsec-scale jet is $\sim 125°$. This might affect the deprojected distance of the jet. However, the jet position angle at the MERLIN scales is still very similar to that in the VLBA scales, so the jet profile between VLBA and MERLIN scales should be compared in the same viewing angle.
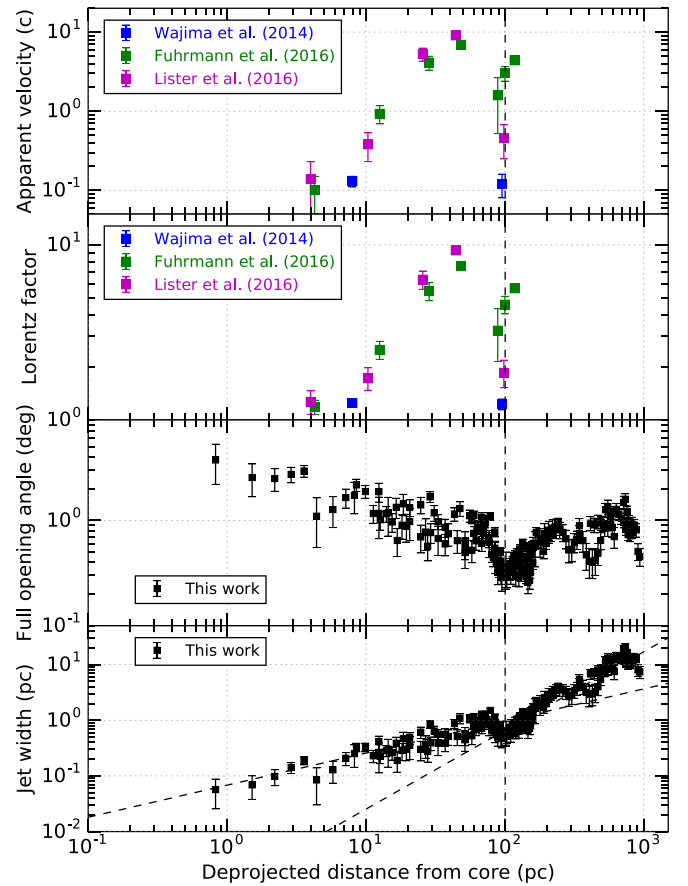

Figure 7. Collimation and acceleration of 1H 0323+342 jet as a function of deprojected distance from the core. A jet viewing angle of 5° is assumed. From top to bottom: Apparent motion reported in the literature, Lorentz factor calculated based on the apparent motion, intrinsic full opening angle calculated from the observed jet width profile, and jet width profile.

including RM measurements would be useful to better understand the B-field properties associated with S.

We also note that the presence of a recollimation shock at some distances from the radio core is also suggested in some other blazars and blazar-like radio galaxies such as 3C 120 (Agudo et al. 2012), 3C 111 (Beuchert et al. 2018), and CTA 102 (Fromm et al. 2011, 2013). In particular, the latter two sources show a peculiar time evolution in radio spectra (CTA 102) or in polarized emission (3C 111) when superluminal components pass through a standing component, which has been interpreted as the interaction of moving shocks with a recollimation shock. Application of a similar multi-epoch analysis to 1H 0323+342 would help confirm the recollimation shock scenario of S and its similarity to blazars.

4.2. Coexistence of Jet Collimation and Acceleration

One of the longstanding central questions regarding relativistic jets is the physical link between collimation and acceleration of the flow. This is vital for understanding the ultimate mechanisms of jet formation (e.g., McKinney 2006; Komissarov et al. 2007) and also the origin/location of γ-ray emission (e.g., Marscher et al. 2008). In recent years, this topic has extensively been examined for the M87 jet (Nakamura & Asada 2013; Asada et al. 2014; Mertens et al. 2016; Hada et al. 2017), and these studies are beginning to uncover the physical link and coexistence of the acceleration and

collimation zone (ACZ) in this jet, which is in agreement with magnetic collimation and acceleration models (e.g., Nakamura et al. 2018). However, very little observational evidence of ACZ has been obtained so far for other sources.

For 1H 0323+342, Fuhrmann et al. (2016), Lister et al. (2016), and Doi et al. (2018) detected significant superluminal motions at parsec scales. Interestingly, they consistently found a trend of a gradual increase of jet proper motion with distance. In addition, the lower brightness temperature of the core than those of typical γ-ray blazars indicates a relatively mild Doppler factor in the core region, suggesting that the innermost jet region is still not fully accelerated (Wajima et al. 2014; Fuhrmann et al. 2016). Therefore, it would be of great interest to compare those velocity results and the collimation profile obtained in our study.

In Figure 7, we show a combined plot of the proper motions in the literature, Lorentz factors (Γ) calculated based on the proper motion results, jet collimation profile, and the corresponding full opening angle profiles as a function of deprojected distance from the core. Here we adopt $\theta_{\mathrm{view}} = 5°$ to calculate the deprojected distance. We also assume that the proper motions traced by jet components reflect bulk flow motions in the jet.

We can indeed see an intriguing signature: the jet kinematics and global jet shape appear to be closely related with each other. The jet speed progressively increases with distance from a few to ≲100 pc, where the jet shape is parabolic and the opening angle smoothly decreases with distance. Then the jet speed becomes the highest (at $\Gamma \sim 10$) immediately before reaching ∼100 pc, where the stationary feature S is located. Beyond this distance, the jet speed seems to be saturated and the jet expands conically. Following M87 (Nakamura & Asada 2013; Asada et al. 2014), this is the second example where the coincidence of collimation and acceleration as well as a recollimation shock at the end of ACZ was discovered.

According to the current theoretical paradigm of powerful AGN jet formation, a jet is initially produced by strong magnetic fields that are amplified by a spinning black hole or/ and the inner part of the accretion disk (Blandford & Znajek 1977; Blandford & Payne 1982). The flow is initially slow in a magnetically dominated state, and the subsequent acceleration is realized by gradually converting the magnetic (and also thermal) energy into kinetic energy, while the ambient pressure from the external medium collimates the flow. As a consequence, an acceleration and collimation zone is co-formed over long distances from the black hole (by either magnetically (McKinney 2006; Komissarov et al. 2007, 2009) or hydrodynamically (Gómez et al. 1997; Perucho & Martí 2007)).

To test whether the observed collimation and acceleration zone in 1H 0323+342 is causally connected, it is important to examine if the product $\Gamma\phi/2$ satisfies the condition $\Gamma\phi/2 \lesssim \sigma_m^{1/2}$, where $\phi/2$ and σ_m is half-opening angle and magnetization parameter of the jet, respectively. This condition can be derived by requiring that the opening angle of a magnetized jet must be smaller than the opening angle of the Mach cone of fast-magnetosonic waves so that the flows can communicate across the jet (Komissarov et al. 2007). If the jet far beyond the central engine is roughly in equipartition (i.e., $\sigma_m \sim 1$), the condition becomes $\Gamma\phi/2 \lesssim 1$. We calculated the product for the five components of Lister et al. (2016), and found $\Gamma\phi/2 \sim (0.01, 0.02, 0.03, 0.04, 0.02)$ for components (6, 5, 4, 3, 2). This indicates that these are all causally well

connected. It is also notable that the values are roughly constant from ∼4 to ∼100 pc, suggesting that the same acceleration/ collimation efficiency is maintained over these distances.

We also note that statistical studies for large samples of blazars indicate $\Gamma\phi/2 \sim 0.2$–0.3 (Clausen-Brown et al. 2013; Jorstad et al. 2017; Pushlarev et al. 2017), a factor of 10 larger than those we estimated in 1H 0323+342. If $\Gamma\phi/2 \sim 0.2$ is the case for 1H 0323+342, this implies that the true bulk flows may be much faster (up to $\Gamma \lesssim 100$) than those suggested in the observed proper motions.

4.3. γ-ray Production at the End of ACZ?

1H 0323+342 exhibits one of most active γ-ray flares among the known γ-ray detected NLS1s (D'Ammando et al. 2016; Paliya et al. 2018), but the exact location of the flaring region is still under debate. In general, active γ-ray emission from AGN jets and blazars is thought to be produced in compact regions near the central engine (≲subparsec scales) due to the observed rapid variability timescales (e.g., Tavecchio et al. 2010). This scenario seems to be favored also for NLS1s based on the modeling of radio-to-γ-ray SED (e.g., Abdo et al. 2009b; Paliya et al. 2014; D'Ammando et al. 2016). As for 1H 0323 +342, Angelakis et al. (2015) report that the source is more variable with higher amplitude at millimeter frequencies than at low frequencies. Indeed, our VLBA 43 GHz image shows that the millimeter-wave emission is dominated by the compact core, and our core-shift measurements suggest that the location of the 43 GHz core is not farther than ∼1 pc from the black hole. This may naturally prefer the scenario that the γ-ray emission from this source is associated with the millimeter-wave core near the black hole.

Nevertheless, our discovery of the extended ACZ with a recollimation shock might propose an alternative scenario for the high-energy site in this source. As also discussed in Doi et al. (2018), the idea is similar to that proposed for HST-1 in M87. The presence of the extended ACZ means that the cross section of the jet remains quite small even at large distances from the black hole. The cross section of S (at $z \sim 100$ pc, deprojected) is still within subparsecs (0.4 pc), with the corresponding intrinsic opening angle reaching minimum at this distance ($\phi \sim 0°.3$). This value of ϕ is much smaller than the averaged ϕ of non-*Fermi*-LAT-detected blazars ($\phi_{\mathrm{LAT}} \sim 2°.5$; Pushlarev et al. 2017) and close to or possibly even smaller than the averaged ϕ of LAT-detected γ-ray blazars ($\phi_{\mathrm{LAT}} \sim 1°.2$; Pushlarev et al. 2017). In fact, Doi et al. (2018) found that the multiple strong γ-ray flaring events that occurred in 2016 (Paliya et al. 2014) coincided with the passage of the fastest superluminal ($\sim 9\,c$) component through the feature S. Interestingly, during this period, this source showed an enhanced power-law X-ray component that was likely from a nonthermal jet, while the thermal emission from the coronal/ disk was relatively low (Paliya et al. 2014). Therefore, one may not preclude the feature S as a potential site of γ-ray emission in 1H 0323+342.

Note that one serious concern for this scenario is that the variability timescale based on the causality argument results in $t_{\mathrm{var}} = R(1 + z)/c\delta \sim 30$ days, which cannot explain the day-scale γ-ray variabilities detected in the previous flares (Paliya et al. 2014). This might be reconciled if the feature S contains more compact substructures like HST-1 (Cheung et al. 2007; Giroletti et al. 2012) or turbulent cells (Marscher 2014), or if the jet contains the faster (larger δ) flows (as discussed in Section 4.2).
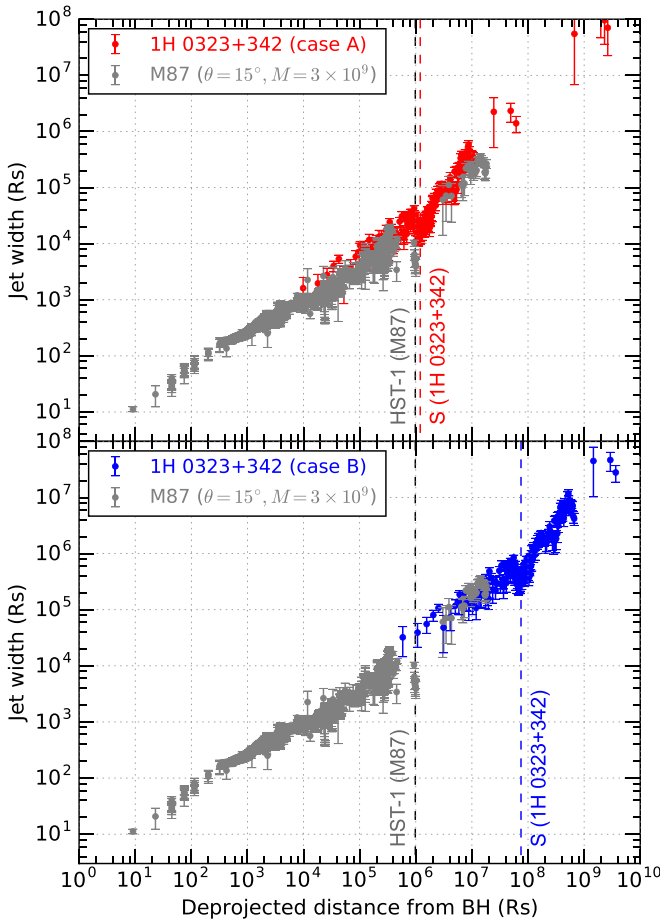
Figure 8. Comparison of the jet collimation profile between 1H 0323+342 and M87 in units of Schwarzschild radius. For 1H 0323+342, we plot two different cases: (A) in red for $(M_{BH}, \theta_{view}) = (4 \times 10^8 M_\odot, 12°)$, and (B) in blue for $(M_{BH}, \theta_{view}) = (2 \times 10^7 M_\odot, 3°)$. The gray data are for M87, which we combined with the results from Asada & Nakamura (2012) and Hada et al. (2013). For M87, $(M_{BH}, \theta_{view}) = (3 \times 10^9 M_\odot, 15°)$ are assumed in this plot. The red and blue vertical dashed lines indicate the distance of S for cases (A) and (B), respectively. The gray vertical dashed line indicates the distance of HST-1.

The production of γ-rays at large distances from the black hole (beyond BLR/torus) is proposed for BL Lacertae (Marscher et al. 2008), PKS 1510-089 (Marscher et al. 2010), and OJ 287 (Agudo et al. 2011) as well as M87/HST-1. These studies all suggest that a recollimation shock that formed at the end of (or beyond) ACZ is a plausible site of γ-ray emission. Some of these studies suggest that γ-ray emission is generated also at another site closer to the central engine (e.g., Hada et al. 2014). In this case, one may expect different patterns of MWL correlation from different γ-ray events. For 1H 0323+342, Paliya et al. (2014) reported that some X-ray events were correlated with γ-rays, while some other X-ray flares had no counterpart in γ-rays, suggesting the existence of multiple high-energy emission sites. A more dedicated VLBI monitoring of this jet and S along with high-energy instruments is the key to unambiguously determine the site(s) of γ-ray production.

4.4. Jet Collimation, Confinement Medium, and Black Hole Mass

The remarkable similarity of the apparent jet structure between 1H 0323+342 and M87 is surprising given the different M_{BH} estimation and different host galaxy type. However, a striking

difference occurs when the spatial scale is measured in R_s units instead of in parsec. Adopting $M_{BH} = 2 \times 10^7 M_\odot$ and $\theta_{view} = 4°–12°$ (Fuhrmann et al. 2016; Lister et al. 2016) for 1H 0323+342, the deprojected distance of the jet transition (i.e., the feature S) from the nucleus results in $(2–9) \times 10^7 R_s$. This is tens to $\sim$100 times more distant than that of HST-1/M87. To maintain a collimated parabola jet shape, pressure support from the external medium is essential (e.g., Komissarov et al. 2007). For M87 (and also NGC 6251 and NGC 4261), the structural transition occurs around $z \sim 10^{5–6} R_s$, which is near the Bondi radius or the sphere of gravitational influence (SGI) of the SMBH (Asada & Nakamura 2012; Tseng et al. 2016; Nakahara et al. 2018). This suggests that the external gas bound by the SMBH potential supports the collimation of these jets.

The discrepancy between 1H 0323+342 and M87 can be reduced if the true M_{BH} of 1H 0323+342 is larger than assumed. Indeed, the exact M_{BH} of this source is still highly controversial: while a small BH mass (a few $\times 10^7 M_\odot$) seems to be generally preferred thanks to the consistency of various different independent methods (Zhou et al. 2007; Wang et al. 2016; Yao et al. 2016; Landt et al. 2017), there are counterarguments suggesting a factor of 10–30 larger M_{BH}, which is typical in blazars (León Tavares et al. 2014). A similar discrepancy of M_{BH} estimation has been observed also for other γ-ray emitting NLS1s FBQS J1644+2619 (D'Ammando et al. 2017) and PKS 2004-447 (Baldi et al. 2016). In Figure 8, we show a plot comparing the jet collimation profiles between M87 and 1H 0323+342 for different M_{BH} and θ_{view}. Interestingly, if we assume $(M_{BH}, \theta_{view}) = (4 \times 10^8 M_\odot, 12°)$ for 1H 0323+342 and $(M_{BH}, \theta_{view}) = (3 \times 10^9 M_\odot, 15°)$ for M87, the jet profiles of the two sources remarkably overlap with each other in R_s unit. This implies a common jet collimation mechanism is at work if M_{BH} of 1H 0323+342 is large. In this case, 1H 0323+342 actually falls onto the famous $M_{BH}–\sigma$ relation ($M_{BH} \propto \sigma^{\sim 4}$; Kormendy & Ho 2013) along with M87. This implies that the SGI, defined by $r_{SGI} = GM_{BH}/\sigma^2$, could be expressed by $r_{SGI} \propto M_{BH}^{\sim 1/2}$. Therefore the collimation of AGN jets from $M_{BH} = 10^{8–9} M_\odot$ might commonly break at distances around $r_{SGI} \sim 3 \times 10^5 R_s$. Note that the jet profile of 1H 0323+342 shown in red in Figure 8 also sufficiently overlaps with those of NGC 6251 (Tseng et al. 2016; Nakamura et al. 2018) and 3C 273 (Akiyama et al. 2018).

On the other hand, if the small M_{BH} is correct, the observed jet collimation would require additional/alternative external support that confines the jet until far beyond the SMBH potential. A likely source of such support would be large-scale winds/outflows surrounding the radio jet. Based on recent radiation-MHD simulations, there are strong indications that super-Eddington BH accretion flows drive powerful outflows due to strong radiation pressure force from the radiatively very efficient accretion flows (Ohsuga et al. 2009; Ohsuga & Mineshige 2011). Recent systematic studies of [O III] emission lines for samples of radio-loud NLS1s have found evidence of powerful outflows (Komossa et al. 2014; Berton et al. 2016b). These outflows are associated with the narrow-line region (NLR), whose spacial scales are assumed to be on the order of 1–100 pc, consistent with the observed collimation scales of 1H 0323+342. Therefore, if the small M_{BH} with high $\dot{M}$ is true for 1H 0323 +342, the observed 1–100 pc scale collimation might be supported by the NLR outflows. Note that the observed NLR outflows in radio-loud NLS1s might also be a consequence of the propagation of relativistic jets rather than driven by the accretion

flows (Berton et al. 2016b). Future VLBI polarimetric observations with RM measurements would provide more insights into the jet-surrounding interactions in this source (e.g., as performed in 3C 120; Gómez et al. 2008, 2012).

Therefore our results on 1H 0323+342 have in any case very intriguing implications for jet collimation, black hole mass, accretion state, confinement medium/environment, and their possible relationship with each other: (1) If the high M_{BH} expected from the M_{BH}–σ relation is the case, the jet collimation may be regulated by the gas bound by the SMBH potential, just as suggested for M87 and nearby radio galaxies. In contrast, (2) if the low M_{BH} (and thus the higher Eddington ratio) is the case, the jet collimation may be regulated by NLR outflows that are driven by super-Eddington BH accretion flows. Solving this question will allow us to build a unified picture of AGN jet formation mechanisms as a function of M_{BH} and $\dot{M}$, and might also help better understand the co-evolution and feedback between SMBH and host galaxies.

5. Summary

We reported results from a detailed nine-frequency VLBA observation of the jet in the nearest γ-ray detected radio-loud NLS1 galaxy 1H 0323+342. We summarize our main results as follows:

1. We obtained multifrequency VLBI images of the 1H 0323+342 jet at various spatial scales from $\sim$100 mas (at 1.4 GHz) down to $\sim$0.1 mas (at 43 GHz). At high frequencies ($\gtrsim$24 GHz), the radio core at the jet base dominates the emission, while at low frequencies ($\lesssim$2 GHz), the quasi-stationary, rebrightened feature S at 7 mas from the core becomes the brightest component. We found that S remained there over more than 10 years.

2. We extensively investigated the width profile $W(z)$ of this jet over a wide range of distance from $z \sim 0.1$ mas to $z \sim 10^4$ mas using our VLBA images and supplementary MERLIN/VLA archival images. We discovered that the jet maintained a parabolic shape from the jet base to $z \sim 7$ mas where S is located, providing evidence of a jet collimation zone. Beyond $z \sim 7$ mas, the jet started to expand more rapidly, transitioning into a hyperbolic/conical shape.

3. We found that the jet cross section of S (i.e., the site of jet transition) is significantly smaller (by a factor of two) than expected from the parabolic profile of the inner jet. Between the inner parabolic zone and the compressed S, we detected a "recollimation zone" connecting these two regions. Moreover, we found that S showed strongly polarized signals (as high as $\sim$30%), possible spectral flattening, and passing of highly superluminal components. A set of these results suggests that the quasi-stationary feature S is a recollimation shock at the end of the collimation zone, producing highly ordered B fields and re-energizing jet particles.

4. By combining the collimation profile and the jet proper motions results in the literature, we discovered the coincidence of jet collimation and acceleration between the jet base and S. The product of Lorentz factor and the (half-) opening angle of this jet satisfies $\Gamma\phi/2 < 1$, indicating that the observed collimation and acceleration zone (ACZ) is causally connected.

5. Our discovery on ACZ showed that the intrinsic opening angle of the jet becomes minimum at S, with the Lorentz factor reaching maximum, suggesting a highly Doppler boosting jet. Together with the fact that an active γ-ray flaring event in 1H 0323+342 coincided with the passage of a highly superluminal component through S (Doi et al. 2018), the recollimation shock S at the end of ACZ might be a potential site of γ-ray production as well as the jet base. The deprojected distance of this feature is $\sim$40–100 pc. The γ-ray production at such distances is much higher than those usually suggested in typical γ-ray blazars, while this situation is quite similar to HST-1 in the jet of M87.

6. We found that the core shift of the 1H 0323+342 jet is small between 1.4 and 43 GHz. This is consistent with the jet having a small viewing angle to our line of sight. We estimated a relative separation between the 43 GHz core and the central BH using the measured parabolic collimation profile of the inner jet, and obtained a deprojected separation of $\sim$(0.24–0.71)pc (or possibly shorter) for a viewing angle of $4°$–$12°$.

7. We found various remarkable similarities in the parsec-scale jet structures between 1H 0323+342 and M87 (e.g., the collimation profile and recollimation shock). If M_{BH} of 1H 0323+342 is $\sim$$4 \times 10^8 M_\odot$ and thus follows the M_{BH}–σ relation, we suggest that a common jet formation mechanism is at work in M87 and 1H 0323+342, where the external gas bound by the SMBH potential plays a role in collimating the jets.

8. If M_{BH} of 1H 0323+342 is a few times $10^7 M_\odot$ (and thus $\dot{M}$ close to or above the Eddington limit), which is proposed by several previous papers, the parabolic jet continues up to $10^{7-8} R_s$ from the black hole, suggesting additional large-scale structures that confine the jet. NLR outflows, which may be driven by super-Eddington accretion flows, could be responsible for the large-scale jet confinement.

Appendix
Calibrator 0329+3510

0329+3510 is a radio source separated by $1°.36$ on the sky from 1H 0323+342. This source is a candidate to be a high-frequency peaker, which is a subclass of young radio galaxies (Dallacasa et al. 2000). In Figure 9 we show self-calibrated images of 0329+3510 obtained at 15, 24, and 43 GHz. The source morphology significantly changes with frequency. At 43 GHz, where the highest angular resolution is available, the source is resolved into the core (the southernmost brightest region) and a strong knot. The core and the knot are also securely resolved at 24 GHz. However, the two features are mixed in a synthesized beam at 15 GHz and the lower
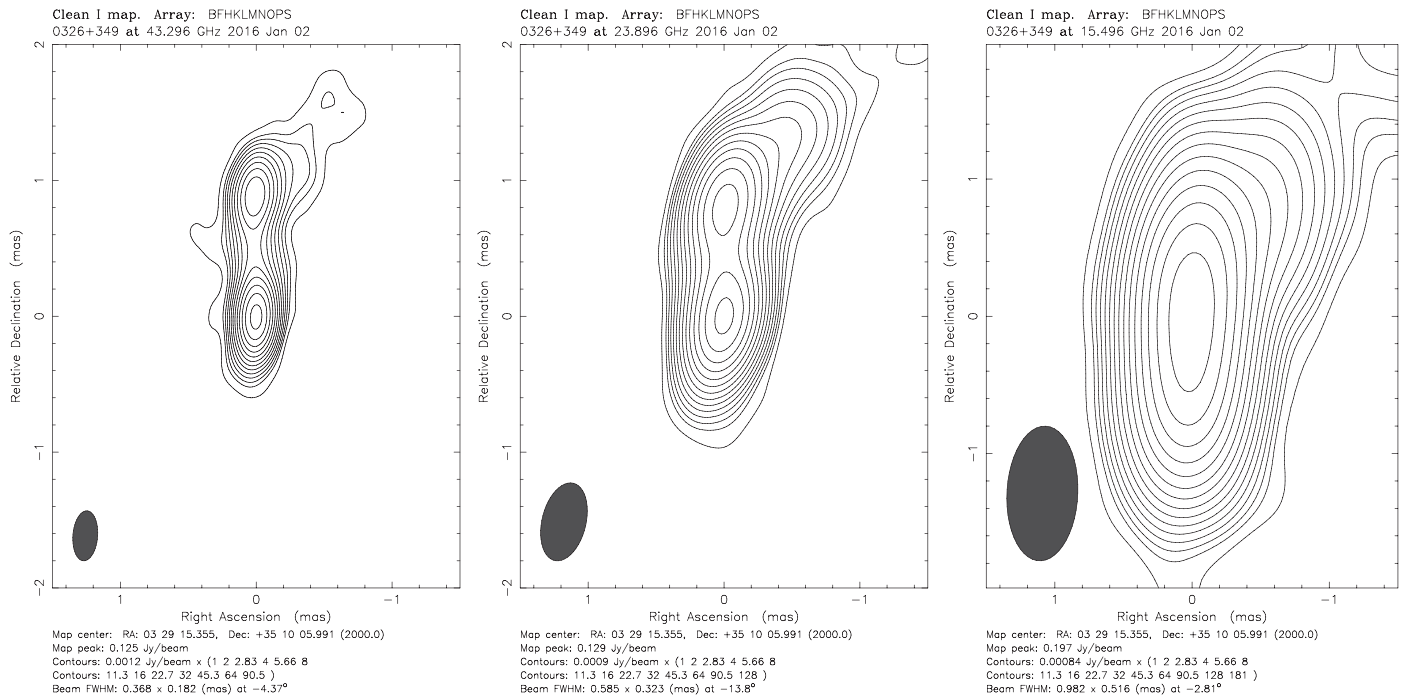
Figure 9. Self-calibrated VLBA images of 0329+3510. From left to right, the images are at 43, 24, and 15 GHz, respectively. For each panel, a restoring beam is shown in the bottom left corner of the map, and contours start from -1, 1, 2, … times a 3σ image rms level and increase by factors of $2^{1/2}$.

frequencies. This is because the knot becomes brighter as frequency decreases (i.e., an optically thin steep spectrum), while the core spectrum is relatively flat or slightly inverted (i.e., optically thick), as well as the resolution effect. This prevents us from specifying a reliable reference position in the 0329+3510 images at $\leqslant$15 GHz.

Therefore, we employed relative astrometry between 1H 0323+342 and 0329+3510 only at 24 and 43 GHz. At each frequency, we measured the core position of 1H 0323 +342 with respect to the core of 0329+3510. In this case, we need to know the effect of the core shift of the calibrator itself since the observed core shift on the target image is a mixture of the core shift from both sources. The source 0329+3510 has a well-defined optically thin knot at 24/43 GHz that should be stationary with frequency, so we can measure the intrinsic core shift of 0329+3510 based on the self-referencing method using the self-calibrated images. As a result, we found that the intrinsic core shift of 0329+3510 between 24 and 43 GHz is virtually negligible (lower than 6 μas). Therefore, the observed core shift of 1H 0323+342 with respect to the core of 0329 +3510 virtually represents the intrinsic core shift of the target.

ORCID iDs

Kazuhiro Hada ⓘ https://orcid.org/0000-0001-6906-772X
Akihiro Doi ⓘ https://orcid.org/0000-0003-4384-9568
Kiyoaki Wajima ⓘ https://orcid.org/0000-0003-3823-7954
Filippo D'Ammando ⓘ https://orcid.org/0000-0001-7618-7527
Marcello Giroletti ⓘ https://orcid.org/0000-0002-8657-8852
Masanori Nakamura ⓘ https://orcid.org/0000-0001-6081-2420

References

Abdo, A. A., Ackermann, M., Ajello, M., et al. 2009a, ApJL, 699, 976
Abdo, A. A., Ackermann, M., Ajello, M., et al. 2009b, ApJL, 707, L142
Agudo, I., Gomeź, J. L., Casadio, C., et al. 2012, ApJ, 752, 92
Agudo, I., Jorstad, S. G., Marscher, A. P., et al. 2011, ApJL, 726, L13
Akiyama, K., Asada, K., Fish, V., et al. 2018, Galax, 6, 15
Angelakis, E., Fuhrmann, L., Marchili, N., et al. 2015, A&A, 575, 55
Antón, S., Browne, I. W. A., & Marchã, M. J. 2008, A&A, 490, 583
Asada, K., Nakamura, M., Doi, A., et al. 2014, ApJL, 781, L2
Asada, N., & Nakamura, M. 2012, ApJL, 745, L28
Baldi, R. D., Capetti, A., Robinson, A., et al. 2016, MNRAS, 458, L69
Berton, M., Caccianiga, A., Foschini, L., et al. 2016a, A&A, 591, 98
Berton, M., Foschini, L., Ciroi, S., et al. 2016b, A&A, 591, 88
Beuchert, T., Kadler, M., Perucho, M., et al. 2018, A&A, 610, A32
Biretta, J. A., Sparks, W. B., & Macchetto, F. 1999, ApJ, 520, 621
Blandford, R. D., & Payne, D. G. 1982, MNRAS, 199, 883
Blandford, R. D., & Znajek, R. L. 1977, MNRAS, 179, 433
Boccardi, B., Krichbaum, T., Bach, U., et al. 2016, A&A, 585, 33
Boller, T., Brandt, W. N., & Fink, H. 1996, A&A, 305, 53
Cheung, C. C., Harris, D. E., & Stawarz, Ł. 2007, ApJL, 663, L65
Clausen-Brown, E., Savolainen, T., Pushkarev, A. B., et al. 2013, A&A, 558, 144
Dallacasa, D., Stanghellini, C., Centonza, M., & Fanti, R. 2000, A&A, 363, 887
D'Ammando, F., Acosta-Pulido, J. A., Capetti, A., et al. 2017, MNRAS, 469, L11
D'Ammando, F., Larsson, J., Finke, J., et al. 2014, MNRAS, 446, 2456
D'Ammando, F., Orienti, M., Finke, J., et al. 2012, MNRAS, 426, 317
D'Ammando, F., Orienti, M., Finke, J., et al. 2013, MNRAS, 436, 191
D'Ammando, F., Orienti, M., Finke, J., et al. 2016, Galax, 4, 11
D'Ammando, F., Orienti, M., Tavecchio, F., et al. 2015, MNRAS, 450, 3975
Deller, A. T., Brisken, W. F., Phillips, C. J., et al. 2011, PASP, 123, 275
Doi, A., Asada, K., & Nagai, H. 2011, ApJ, 738, 126
Doi, A., Fujisawa, K., Inoue, M., et al. 2007, PASJ, 59, 703
Doi, A., Hada, K., Kino, M., et al. 2018, ApJL, 857, L6
Doi, A., Nagai, H., Asada, K., et al. 2006, PASJ, 58, 829
Foschini, L., Ghisellini, G., Kovalev, Y. Y., et al. 2011, MNRAS, 413, 1671
Fromm, C. M., Ros, E., Perucho, M., et al. 2011, A&A, 531, 95
Fromm, C. M., Ros, E., Perucho, M., et al. 2013, A&A, 551, 32
Fuhrmann, L., Karamanavis, V., Komossa, S., et al. 2016, RAA, 16, 176
Gallo, L. C., Edwards, P. G., Fererro, E., et al. 2006, MNRAS, 370, 245
Giovannini, G., Savolainen, T., Orienti, M., et al. 2018, NatAs, 2, 472
Giroletti, M., Hada, K., Giovannini, G., et al. 2012, A&A, 538, L10
Giroletti, M., Paragi, Z., Bignall, H., et al. 2011, A&A, 528, L11
Gómez, J. L., Lobanov, A. P., Bruni, G., et al. 2015, ApJ, 817, 96
Gómez, J. L., Marscher, A. P., Jorstad, S. G., et al. 2008, ApJL, 681, L69
Gómez, J. L., Martí, J. M., Marscher, A. P., et al. 1997, ApJL, 482, L33

Gómez, J. L., Roca-Sogorb, M., Agudo, I., et al. 2012, ApJ, 733, 11
Hada, K., Doi, A., Kino, M., et al. 2011, Natur, 477, 185
Hada, K., Giroletti, M., Giovannini, G., et al. 2015, arXiv:1504.01808
Hada, K., Giroletti, M., Kino, M., et al. 2014, ApJ, 788, 165
Hada, K., Kino, M., Doi, A., et al. 2013, ApJ, 775, 70
Hada, K., Kino, M., Doi, A., et al. 2016, ApJ, 817, 131
Hada, K., Park, J.-H., Kino, M., et al. 2017, PASJ, 69, 71
Itoh, R., Tanaka, Y. T., Akitaya, H., et al. 2014, PASJ, 66, 108
Jorstad, S. G., Marscher, A. P., Morozova, D. A., et al. 2017, ApJ, 846, 98
Kynoch, D., Landt, H., Ward, M. J., et al. 2018, MNRAS, 475, 404
Komissarov, S. S., Barkov, M. V., Vlahakis, N., & Königl, A. 2009, MNRAS,
    394, 1182
Komissarov, S. S., Vlahakis, N., & Königl, A. 2007, MNRAS, 380, 51
Komossa, S., Xu, D., & Zensus, A. 2014, in IAU Symp. 312, Star Clusters and
    Black Holes in Galaxies Across Cosmic Time, ed. Y. Meiron et al. (San
    Francisco, CA: ASP), 63
Kormendy, J., & Ho, L. 2013, ARA&A, 51, 511
Kotilainen, J. K., León-Tavares, J., Olguín-Iglesias, A., et al. 2017, ApJ,
    832, 157
Landt, H., Ward, M. J., Baloković, M., et al. 2017, MNRAS, 464, 2564
León Tavares, J., Kotilainen, J., Chavushyan, V., et al. 2014, ApJ, 795, 58
Lister, M. L., Aller, H. D., Aller, M. F., et al. 2009, AJ, 137, 3718
Lister, M. L., Aller, M. F., Aller, H., et al. 2016, AJ, 152, 12
Lobanov, A. P. 1998, A&A, 330, 79
Marscher, A. P. 2014, ApJ, 780, 87
Marscher, A. P., Jorstad, S. G., D'Arcangelo, F. D., et al. 2008, Natur, 452, 966
Marscher, A. P., Jorstad, S. G., Larionov, V. M., et al. 2010, ApJL, 710, L126

McKinney, J. C. 2006, MNRAS, 368, 1561
Mertens, F., Lobanov, A. P., Walker, R. C., & Hardee, P. E. 2016, A&A,
    595, A54
Nagai, H., Haga, T., Giovannini, G., et al. 2014, ApJ, 785, 53
Nakahara, S., Doi, A., Murata, Y., et al. 2018, ApJ, 854, 148
Nakamura, M., & Asada, K. 2013, ApJ, 775, 118
Nakamura, M., Asada, K., Hada, K., et al. 2018, ApJ, submitted
Ohsuga, K., & Mineshige, S. 2011, ApJ, 736, 2
Ohsuga, K., Mineshige, S., Mori, M., et al. 2009, PASJ, 61, L7
Orienti, M., D'Ammando, F., Giroletti, M. & for the Fermi-LAT Collaboration
    2012, arXiv:1205.0402
Orienti, M., D'Ammando, F., Larsson, J., et al. 2015, MNRAS, 453, 4037
Osterbrock, D. E., & Pogge, R. W. 1985, ApJ, 297, 166
Paliya, V. S., Ajello, M., Rakshit, S., et al. 2018, ApJL, 853, L2
Paliya, V. S., Sahayanathan, S., Parker, M. L., et al. 2014, ApJ, 789, 143
Perucho, M., & Martí, J. M. 2007, MNRAS, 382, 526
Pushlarev, A. B., Kovalev, Y. Y., Lister, M., et al. 2017, MNRAS, 468,
    4992
Shepherd, M. C. 1997, in ASP Conf. Ser. 125, Astronomical Data Analysis
    Software and Systems VI, ed. G. Hunt & H. E. Payne (San Francisco, CA:
    ASP), 77
Tavecchio, F., Ghisellini, G., Bonnoli, G., et al. 2010, MNRAS, 405, L94
Tseng, C.-Y., Asada, K., Nakamura, M., et al. 2016, ApJ, 833, 288
Wajima, K., Fujisawa, K., Hayashida, M., et al. 2014, ApJ, 781, 75
Wang, F., Du, P., Hu, C., et al. 2016, ApJ, 824, 149
Yao, S., Yuan, W., Komossa, S., et al. 2016, AJ, 150, 23
Zhou, H.-Y., Wang, T.-G., Yuan, W.-M., et al. 2007, ApJL, 658, L13